Journal of Solid State Chemistry 184 (2011) 1924–1930

Contents lists available at ScienceDirect

Journal of Solid State Chemistry

journal homepage: www.elsevier.com/locate/jssc

Design of highly ordered Ag–$SrTiO_3$ nanotube arrays for photocatalytic degradation of methyl orange

Yue Sun [a], Jiawen Liu [a,*], Zhonghua Li [b,**]

[a] Key Laboratory of Design and Synthesis of Functional Materials and Green Catalysis, Colleges of Heilongjiang Province, College of Chemistry and Chemical Engineering, Harbin Normal University, Harbin 150025, PR China

[b] Key Laboratory of Microsystems and Microstructures Manufacturing, Ministry of Education, Harbin Institute of Technology, Harbin 150001, PR China

ARTICLE INFO

Article history:
Received 28 January 2011
Received in revised form
25 April 2011
Accepted 29 May 2011
Available online 6 June 2011

Keywords:
Ag–$SrTiO_3$ nanotube arrays
Photocatalyst
Degradation
Methyl orange

ABSTRACT

Ag–$SrTiO_3$ nanotube arrays were successfully prepared for the degradation of methyl orange (MO) under ultraviolet irradiation. In order to form highly ordered $SrTiO_3$ nanotube arrays, the preparation of TiO_2 nanotube arrays by anodic oxidation of titanium foil in different electrolytes was investigated. The selected organic solvents in electrolytes include glycerol, dimethyl sulfoxide and glycol. The results indicate that the morphology of TiO_2 nanotube arrays prepared in glycol containing ammonium fluoride electrolyte is more regular. Then $SrTiO_3$ nanotube arrays were synthesized by a hydrothermal method using TiO_2 nanotube arrays as the precursor. In order to further improve the photocatalytic activity of $SrTiO_3$ nanotube arrays, Ag nanoparticles were loaded on $SrTiO_3$ nanotube arrays by two sets of experiments. The loaded Ag results in an enhancement of photocatalytic activity of $SrTiO_3$ nanotube arrays. Moreover, the effect of pH on the photocatalytic degradation of MO was also studied.

1. Introduction

Functional nanomaterials have become a research hotspot in recent years as result of their surface effects, small size effects, quantum tunneling effects and other novel features. In particular, nanomaterials with special structures such as nanotubes, nanowires, nanorods, etc., reflect the superiority of catalysis applications [1–3]. Facing the urgent problems of energy requirement and environmental purification in the industrialized world, applications of nanomaterials in photocatalytic hydrogen evolution [4–6] and photocatalytic degradation of organic pollutants [7] have received great attention. Semiconductor photocatalysts play a major role in photocatalysis. Among them, nanostructured TiO_2 is one of the most promising photocatalytic materials. To date, most of the investigations on photocatalysis have focused on enhancing the photocatalytic activity of TiO_2 [8–10]. However, the design and development of novel nanostructured photocatalysts is also research focus. Recently, perovskite strontium titanate ($SrTiO_3$) has been investigated due to its ferroelectricity, superconductivity, high dielectric constant, and thermal stability [11,12]. In addition, $SrTiO_3$ is one of important photocatalysts and has been used for water splitting and degradation of organic compounds under ultraviolet (UV) radiation [13–16]. Though the formation of nanotube materials has been widely studied [17–20], the preparation of nanotube arrays with perovskite structure (ABO_3) remains a challenge in materials science [21–24]. The main challenge is to keep the high order array morphology from disorder during the synthesis process [23]. In the present work, we prepared highly ordered $SrTiO_3$ nanotube arrays by the hydrothermal method on the basis of TiO_2 nanotube arrays obtained by anodic oxidation method. The highly ordered $SrTiO_3$ nanotube arrays with one-dimensional structure are easier for the transfer of charge carriers than particulate catalyst and thus reduce the loss of charge carriers. Moreover, Ag–$SrTiO_3$ nanotube arrays were prepared by photochemistry reduction. The presence of Ag nanoparticles as electrons receiver can effectively separate the electrons and holes, and so the efficiency of catalytic redox reactions can be further enhanced [25].

2. Experimental

2.1. Preparation of photocatalysts

Titanium foils (99.5% purity) were cut into 2 cm × 4 cm in size, and mechanically burnished with different abrasive papers. Hereafter, Ti foils were cleaned by sonication in acetone and distilled water, and dried in air. Then the cleaned Ti foils were chemically etched by immersing in a mixed acid solution (the mixing ratio of $HF/HNO_3/H_2O$ was 1:4:5 in volume, respectively), followed

* Corresponding author. Fax: +86 451 88060851.
** Corresponding author.
E-mail addresses: jiawenliu@yahoo.com.cn, jwliu@hrbnu.edu.cn (J. Liu), lizh@hit.edu.cn (Z. Li).

0022-4596/$ - see front matter © 2011 Elsevier Inc. All rights reserved.
doi:10.1016/j.jssc.2011.05.037

Table 1
Detailed experimental conditions for the preparation of samples.

TiO_2 sample	Electrolyte composition	Voltage (V)	$SrTiO_3$ sample	Hydrothermal time (h)
T1	Glycerol + H_2O(4:1) + 0.5 wt% NH_4F	30	S1	2
			S1	10
T2	Glycerol + H_2O(1:1) + 0.5 wt% NH_4F	20		
T3	Glycerol + DMSO + H_2O(9:1:1) + 0.5 wt% NH_4F	30		
T4	Glycol + 3.0 wt% H_2O + 0.5 wt% NH_4F	60	S4	2
			S4	10

by rinsing with distilled water and drying in air. Titanium dioxide nanotubes were prepared from Ti foils by anodization using another titanium sheet as a counter electrode. The distance between the anode and cathode was 5 cm. Anodization experiments were carried out in different electrolytes and voltages. The electrolyte composition and voltage used for anodization are listed in Table 1. TiO_2 nanotube arrays were prepared by two-step anodization process. The first anodization was performed for 30 min, and then the formed TiO_2 thin film was removed by ultrasonic rinse in hydrochloric acid. The second anodization was then performed for 1 h to form highly ordered TiO_2 nanotube arrays.

The $SrTiO_3$ nanotube arrays were formed by hydrothermal method using TiO_2 nanotube arrays as templates. The prepared TiO_2 samples were immersed in 0.05 M strontium hydroxide solutions. Then the reaction was conducted in a Teflon reactor at 150 °C for different durations (2 and 10 h). Following the samples were removed from the solution, cleaned and dried.

In order to compare with the nanotube array film, the commercial TiO_2 and $SrTiO_3$ particle films on titanium substrate were prepared. $SrTiO_3$ particles were synthesized by solvothermal method [13]. Then 0.01 g TiO_2 or $SrTiO_3$ powder was dispersed in 2 mL distilled water by ultrasonic vibration. The obtained solution was uniformly painted on titanium foil. Finally, the sample was dried.

The Ag loaded $SrTiO_3$ nanotube arrays were prepared by photochemistry reduction method. Two different preparation methods were carried out to obtain Ag loaded $SrTiO_3$ nanotube arrays. One is that $SrTiO_3$ nanotube arrays were immersed in 0.5 M $AgNO_3$ solution at 60 °C for 24 h. Then, the prepared samples were irradiated by a 350 W high-pressure Hg lamp (λ_{max}=365 nm) for 1 h in 40 ml methanol. The other one is that $SrTiO_3$ nanotube arrays were directly irradiated for 3 h in 0.5 M $AgNO_3$ solution. The Ag loaded $SrTiO_3$ nanotube arrays obtained by the above preparation methods were further investigated.

2.2. Characterization

The surface morphology and composition of the samples were investigated by field-emission scanning electron microscopy (FE-SEM; HITACHI S-4800) with energy dispersive X-ray (EDX) spectroscopy. The crystalline structure of the samples was determined by an X-ray diffraction (XRD) using a Rigaku D/MAX-RB diffractometer with Cu $K\alpha$ radiation. X-ray photoelectron spectroscopy (XPS) measurement was carried out on a PHI 5700 ESCA System with an Al $K\alpha$ X-ray source. After photocatalytic degradation, the absorbance values of methyl orange were measured with a Perkin Elmer Lambda 45 UV/VIS Spectrometer and an ultraviolet-visible (UV–vis) spectrophotometer-722M.

2.3. Photocatalytic activity

The photocatalytic activity of the samples was evaluated by the photocatalytic degradation of methyl orange (MO) aqueous solution. The initial concentration of MO solution was 20 mg/L and the desired pH value of MO solution was adjusted with HCl solution. The experiment of photocatalysis was performed in a quartz reactor using a 350 W high-pressure Hg lamp as light source, which was positioned at 10 cm away from the quartz reactor. The photocatalytic test was performed at room temperature. To keep the reaction temperature constant, recycled cooling water was used in the quartz reactor. The nanotube array film was immersed in 100 mL MO aqueous solution. The solution was first stirred in the dark for 30 min to reach the adsorption equilibrium before irradiation. After ultraviolet light irradiation, the reaction solution was periodically taken from the reactor for the determination of the absorbance change of MO and analyzed by an UV–vis spectrophotometer. During this process the solution was continuously stirred. The selected analytic wavelengths were 508 nm at pH 3 and 464 nm at pH 7. For comparison, the blank test was also carried out by irradiating MO homogeneous solution without photocatalyst for checking the self-photolysis of MO.

3. Results and discussion

3.1. Preparation of TiO_2 nanotube arrays

Fig. 1 shows the scanning electron microscopy images of titanium surface films anodized under different preparation conditions. The anodization conditions are listed in Table 1. The samples were labeled as T1, T2, T3 and T4. From Fig. 1 it can be seen that self-organized TiO_2 nanotubes can be formed in all investigated electrolytes, but the morphologies of the nanotube arrays are different. Fig. 1a displays that the morphology of TiO_2 nanotube arrays (T1) is not enough regular, the diameter size is non-uniform and the nozzles are not round. For T2 as shown in Fig. 1b, the morphology of the nanotube arrays is slightly improved, but there are some fragmentized nanotubes on the surface of the sample. Fig. 1c shows the morphology of T3. Due to the presence of dimethyl sulfoxide (DMSO), the nanotubes tend to be round and uniform in diameter. However, the arrays become a little loose and scraggly. In order to obtain regular arrays of oriented nanotubes, a low-viscosity electrolyte was used, namely, the electrolyte is glycol solution containing 0.5 wt% NH_4F and 3.0 wt% distilled water. It is apparent that highly ordered nanotube arrays with uniform diameter are formed as shown in Fig. 1d. The nozzles of the nanotubes are open on the top and very round. Moreover, the arrangement of the nanotubes is regular and compact. The average internal diameter of these nanotubes is about 110 nm with wall thickness of about 12 nm.

3.2. Formation of $SrTiO_3$ nanotube arrays

3.2.1. Morphology of $SrTiO_3$ nanotube arrays

In order to form highly ordered $SrTiO_3$ nanotube arrays, the samples of T1 and T4 were treated by hydrothermal method. At first, T1 and T4 were heat-treated at 150 °C for 2 h, the obtained samples were labeled as S1-2 and S4-2, respectively. Fig. 2a and b shows the SEM images of S1-2 and S4-2. It is found that after

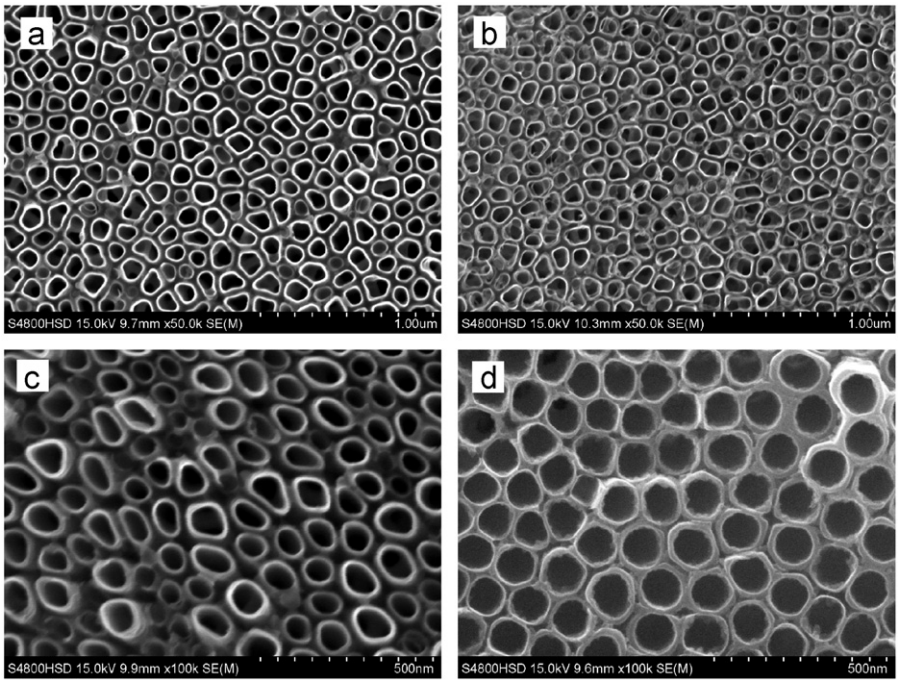

Fig. 1. Morphologies of TiO_2 nanotube arrays fabricated by anodization in different electrolytes: (a) T1, (b) T2, (c) T3 and (d) T4.

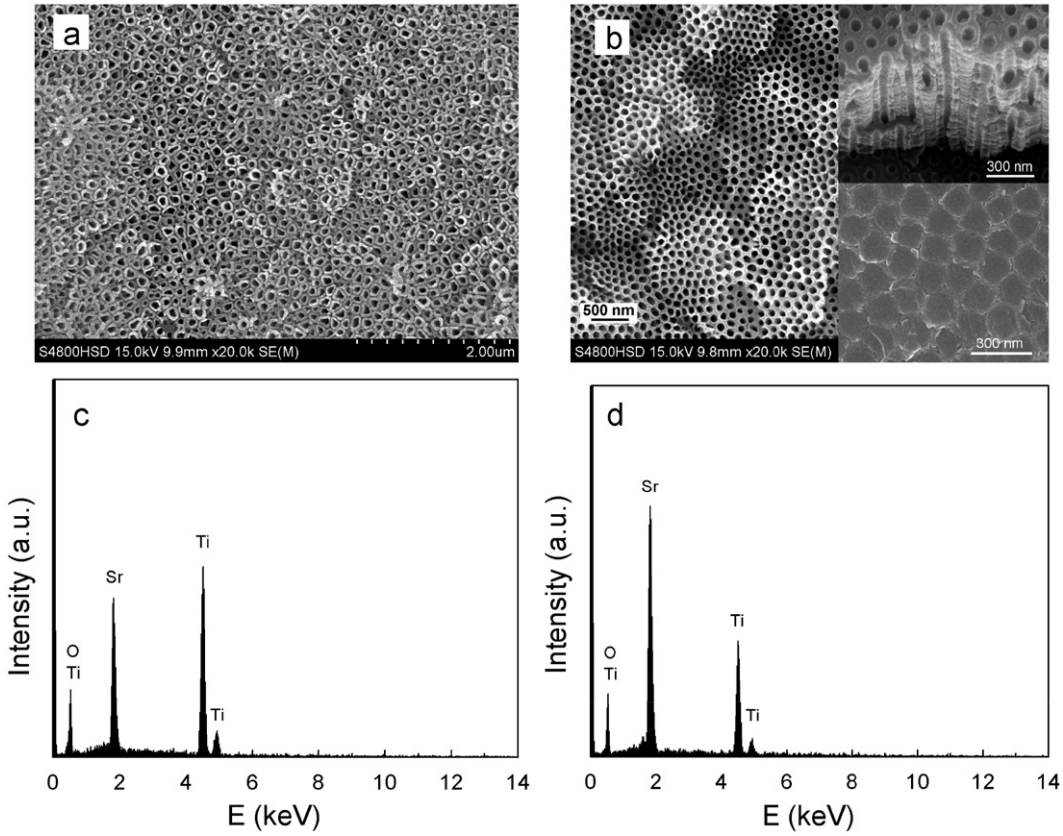

Fig. 2. SEM images: (a) S1-2 and (b) S4-2, the insets show the top-view and the bottom-view; EDX spectra: (c) S1-2 and (d) S4-2.

hydrothermal treatment, the morphologies of samples have no obvious change compared with T1 and T4, except that the wall thickness of the nanotubes is slightly increased due to the crystal cell expansion. The tubular structure for the sample S1-2 is still irregular as shown in Fig. 2a. For the sample S4-2, the nanotubes are very uniform, smooth and round as shown in Fig. 2b. The average internal diameter of these nanotubes is about 90 nm with wall thickness about 24 nm. The inset in Fig. 2b shows the SEM images of the side-view of mechanical destruction nanotubes and the bottom-view. It can be seen that these nanotubes are all straight, parallel

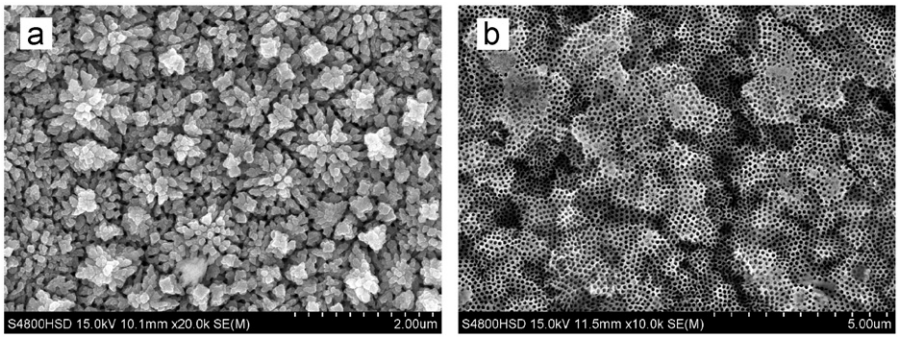

Fig. 3. SEM images of (a) S1-10 and (b) S4-10.

and closely connected to each other. The nanotube bottoms have round shapes and the outer diameter of the nanotubes is very uniform.

The composition elements of S1-2 and S4-2 were determined by energy dispersive X-ray (EDX) analysis. The results reveal that Ti, O and Sr are the composition elements of the samples (Fig. 2c and d). The atomic percent of Sr is 8.49 and 15.92 for S1-2 and S4-2, respectively. However, the atomic percent of Ti in S1-2 (28.47) is higher than that in S4-2 (19.76). This may be due to the layer thickness and the bottom layer thickness increase with increasing voltage from 30 to 60 V. Therefore, the ratio of $SrTiO_3$ layer to Ti substrate in S4-2 is higher, resulting in the higher atomic percent of Sr in EDX.

In order to study the effect of reaction time on the morphology of $SrTiO_3$ nanotube arrays, T1 and T4 were heat-treated at 150 °C for 10 h, the obtained samples were labeled as S1-10 and S4-10, respectively. Fig. 3a shows the SEM image of S1-10. It is found that the reaction time has a significant influence on the morphology of $SrTiO_3$ nanotube arrays obtained from T1. The wall thickness would become thicker if the reaction time is increased and the morphology of many nanotubes has been destroyed. However, the nanotube arrays morphology of S4-10 is still very ordered as shown in Fig. 3b. Compared with S4-2, no obvious changes are observed. The morphologies of S4-2 and S4-10 are very similar. This indicates that nanotube structures obtained from T4 are very stable. Moreover, the above experimental results indicate that although TiO_2 nanotube arrays can be prepared successfully in different electrolytes and at different voltages, the effects of different anodization conditions on the microstructure of $SrTiO_3$ nanotube arrays obtained from anodized TiO_2 nanotubes are different. This may be related to the initial structure of TiO_2 nanotubes.

3.2.2. The XRD analysis of $SrTiO_3$ nanotube arrays

Fig. 4 shows the XRD pattern of $SrTiO_3$ nanotube arrays prepared by hydrothermal method at 150 °C for 2 h (S4-2) and 10 h (S4-10). All of their characteristic peaks, which represent the phase formation of $SrTiO_3$ are in good agreement with a cubic perovskite structure of $SrTiO_3$ (JCPDS Card no. 40-1500). The peaks of Ti are inevitable due to the thinner film and its porous structure. Moreover, the cubic $SrTiO_3$ could be successfully synthesized from TiO_2 template by hydrothermal treatment for 2 or 10 h. In the following experiments, $SrTiO_3$ nanotube arrays used to load silver nanoparticles were prepared by hydrothermal method at 150 °C for 2 h.

3.3. Formation of Ag–$SrTiO_3$ nanotube arrays

3.3.1. Morphology of Ag–$SrTiO_3$ nanotube arrays

After $SrTiO_3$ nanotube arrays were successfully prepared, two sets of experiments were designed to load Ag on the $SrTiO_3$ nanotubes. In the first set, the $SrTiO_3$ nanotube arrays were put into 0.5 M $AgNO_3$ solution, and then the solution was irradiated by a 350 W high-pressure Hg lamp for 3 h, the obtained sample was labeled as SA1. Fig. 5a shows the SEM image of SA1. From Fig. 5a it can be seen that there is almost no Ag nanoparticles on the nanotubes. This was confirmed by the energy spectrum analysis in Fig. 5b. In the second set, after the $SrTiO_3$ nanotube arrays were immersed in 0.5 M $AgNO_3$ solution for 24 h, photochemistry reduction was carried out for 1 h in 40 mL methanol. The obtained sample was labeled as SA2. The SEM image of SA2 is shown in Fig. 5c. As can be seen from Fig. 5c, Ag nanoparticles are obviously loaded on the nanotubes and the presence of Ag nanoparticles does not destroy the morphology of $SrTiO_3$ nanotube arrays. The energy spectrum analysis in Fig. 5d also reveals that, besides Ti, O and Sr, Ag is also the main element of the sample. Therefore, the Ag–$SrTiO_3$ nanotube arrays were synthesized successfully.

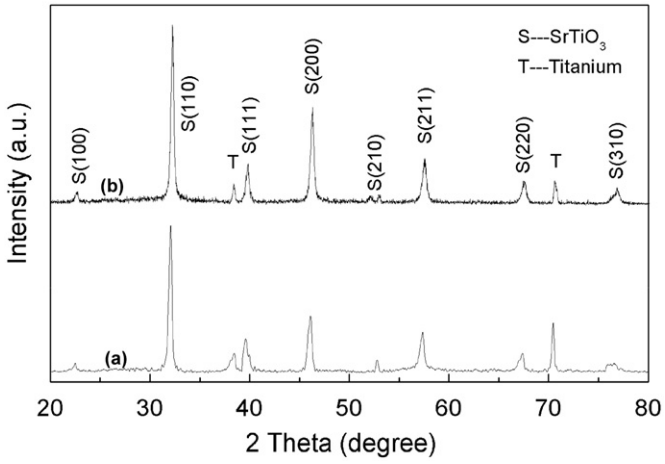

Fig. 4. X-ray diffraction patterns of $SrTiO_3$ nanotube arrays: (a) S2 and (b) S4.

3.3.2. The XRD analysis of Ag–$SrTiO_3$ nanotube arrays

The XRD pattern of Ag–$SrTiO_3$ nanotube arrays obtained after photochemistry reduction is shown in Fig. 6a. Compared with Fig. 4, an additional phase was identified to be the Ag (JCPD card no. 04-0783). The peak at $2\theta = 38.1^\circ$ is characteristic of Ag metal, which confirms the deposition of Ag on $SrTiO_3$ nanotube arrays. However, the peak of Ag (111) observed at $2\theta = 38.1^\circ$ overlaps with the Ti peak. In addition, Ag–$SrTiO_3$ nanotube arrays obtained after degradation of methyl orange was also characterized by XRD, as shown in Fig. 6b. Compared with Fig. 6a, it is found that there is no structural change before degradation and after degradation. Photodegradation did not affect the Ag and $SrTiO_3$

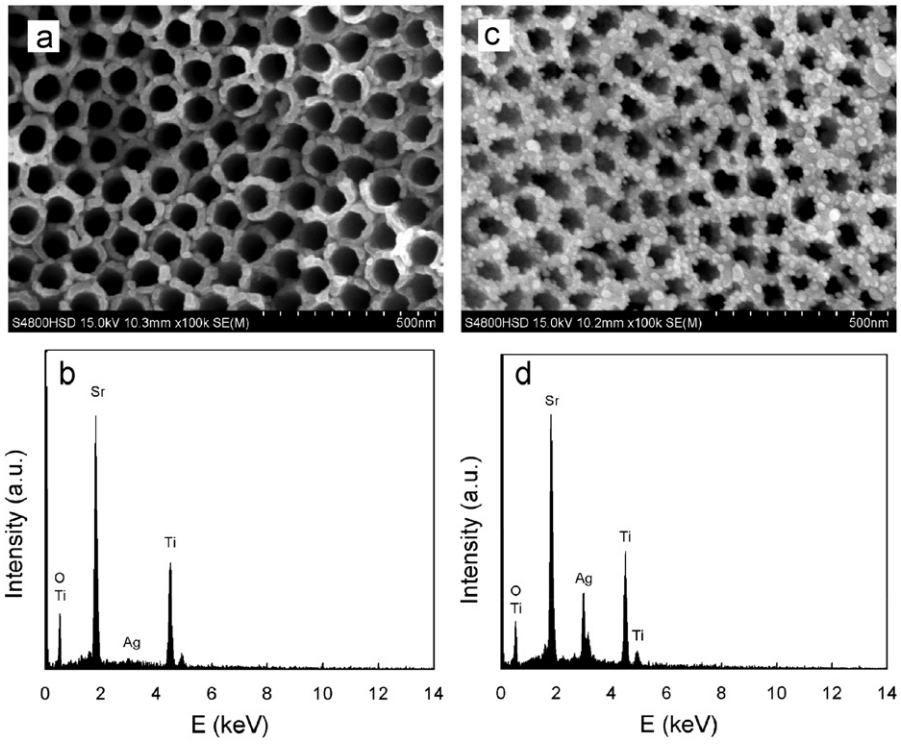

Fig. 5. SEM images: (a) SA1 and (c) SA2; EDX spectra: (b) SA1 and (d) SA2.

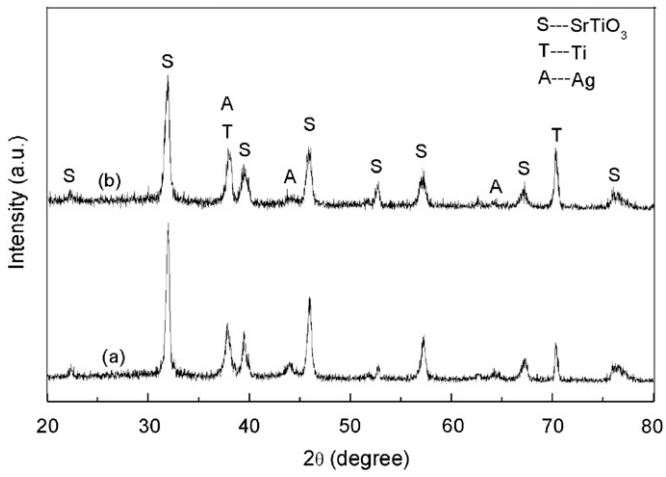

Fig. 6. X-ray diffraction patterns of Ag–$SrTiO_3$ nanotube arrays: (a) before degradation and (b) after degradation.

phases. Ag particles remain the cubic metallic Ag, and $SrTiO_3$ nanotubes remain the cubic perovskite structure. The result indicates that photocatalytic degradation of methyl orange has no effect on the structure of the catalyst.

3.3.3. *The XPS analysis of Ag–$SrTiO_3$ nanotube arrays*

To affirm the composition and chemical state of elements on the surface of samples, the Ag–$SrTiO_3$ nanotube arrays were further characterized by XPS, and the results are shown in Fig. 7. The wide-scan XPS spectrum reveals that Ag–$SrTiO_3$ nanotube arrays contain Ag, Sr, Ti, O and C, as shown in Fig. 7a, while C element mainly come from atmospheric contamination adsorbed on the surface of Ag–$SrTiO_3$ nanotube arrays. The binding energies of the XPS spectra were calibrated by C1s (285.0 eV). Fig. 7b shows the high-resolution XPS spectrum of

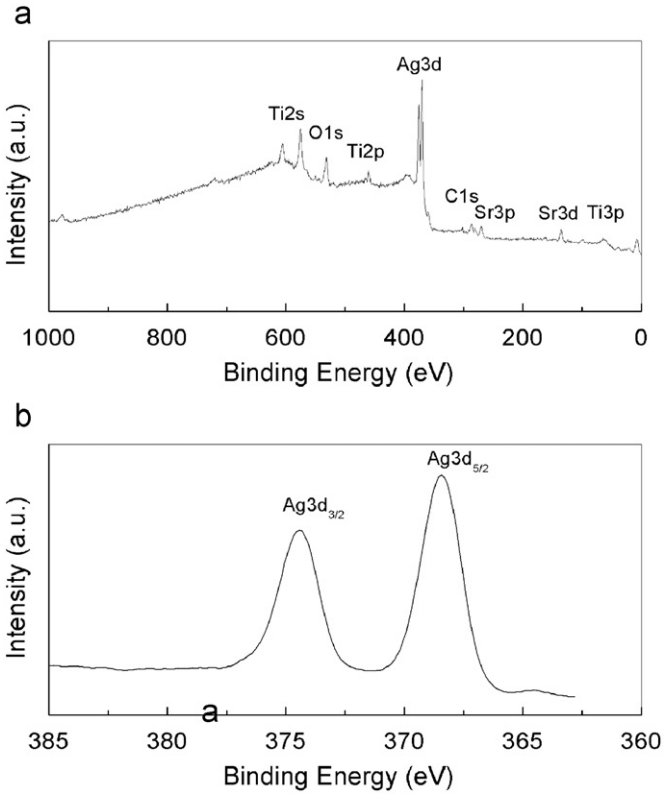

Fig. 7. XPS spectra of Ag–$SrTiO_3$ nanotube arrays: (a) the wide-scan XPS spectrum and (b) the high-resolution Ag 3d spectrum.

Ag 3d. It exhibits two peaks at 368.4 and 374.4 eV, which is attributed to Ag $3d_{5/2}$ and Ag $3d_{3/2}$ binding energies, respectively. The result confirms that the deposited Ag exists in the Ag^0 state on the $SrTiO_3$ nanotube arrays [26].

3.3.4. Formation mechanism of Ag–$SrTiO_3$ nanotube arrays

The synthesis of Ag–$SrTiO_3$ nanotube arrays is schematically presented in Fig. 8. Firstly, highly ordered TiO_2 nanotube arrays were synthesized by anodic oxidation, and then $SrTiO_3$ nanotube arrays were formed by hydrothermal method using TiO_2 nanotube arrays as templates. Following the $SrTiO_3$ nanotube arrays were immersed in $AgNO_3$ solution in order to make the solution substantially enter into the nanotubes. After photochemistry reduction, the Ag–$SrTiO_3$ nanotube arrays were obtained.

3.4. Photocatalytic activity of Ag–$SrTiO_3$ nanotube arrays

The photocatalytic activity of Ag–$SrTiO_3$ nanotube arrays was examined by monitoring the degradation of methyl orange. Effect of pH value on the degradation of methyl orange was also investigated. Fig. 9a and b presents the relationship between the irradiation time and the degradation rate of methyl orange catalyzed by Ag–$SrTiO_3$ nanotube arrays at pH 3 and 7, respectively. In Fig. 9a and b, C_0 is the initial concentration of MO, and C is the concentration of MO after UV light irradiation. For the studied dyes, the blank experiments were investigated in the absence of photocatalyst. From Fig. 9a, it can be seen that almost no MO degradation occurs at pH 7, while Fig. 9b shows that only a small quantity of MO is degraded at pH 3. This can be explained by the change of the molecular structure of MO. The molecular structure of MO changes from an azo type in the neutral solution to a quinoid type in the acidic solution. So, MO in acidic condition is easier to be degraded than in neutral condition due to the decrease of conjugate system [27].

For comparison, the photocatalytic activities of TiO_2 and $SrTiO_3$ particle film were also presented. The result indicates that the photocatalytic activity of $SrTiO_3$ nanotube arrays is significantly higher than those of TiO_2 and $SrTiO_3$ particle film as shown in Fig. 9. Moreover, the Ag–$SrTiO_3$ nanotube arrays achieve the best performance for MO photodegradation. The photocatalytic activity of $SrTiO_3$ nanotube arrays is greatly improved by loading Ag. The excellent photocatalytic activity of Ag–$SrTiO_3$ nanotube arrays is attributed to the modification of silver, which can restrain the recombination of photogenerated electron–hole pairs by Schottky junctions at Ag/$SrTiO_3$ interface [28].

Compared with Fig. 9a, the photocatalytic degradation rate of MO at pH 3 is faster than that at pH 7 as shown in Fig. 9b. The MO dye is almost completely decomposed by Ag–$SrTiO_3$ nanotube arrays after irradiation 60 min at pH 3. However, the degradation rate of MO only can reach 40% after irradiation 120 min at pH 7. This indicates that pH value is also one of the factors influencing the degradation rate, and acidic conditions are very favorable for the degradation of methyl orange. This is due to that pH value influences the surface charge of $SrTiO_3$ catalyst and the adsorption of organic compounds onto the $SrTiO_3$ surface, and the concentration of the hydroxyl radicals. It is well known that methyl orange is an anionic dye and the surface of $SrTiO_3$ is positively charged at low pH values. Therefore, the methyl orange ion is easy to be adsorbed by $SrTiO_3$ catalyst due to the increase of induced interaction. In addition, the number of •OH radical with high oxidative activity on the surface of $SrTiO_3$ increases by trapping photons at low pH values [29]. However, at high pH values, the interaction between the negatively charged surface of $SrTiO_3$ and MO ion is the Coulombic repulsion, resulting in the decreasing of adsorption. Therefore, Ag–$SrTiO_3$ nanotube arrays show higher photocatalytic activity at a low pH value.

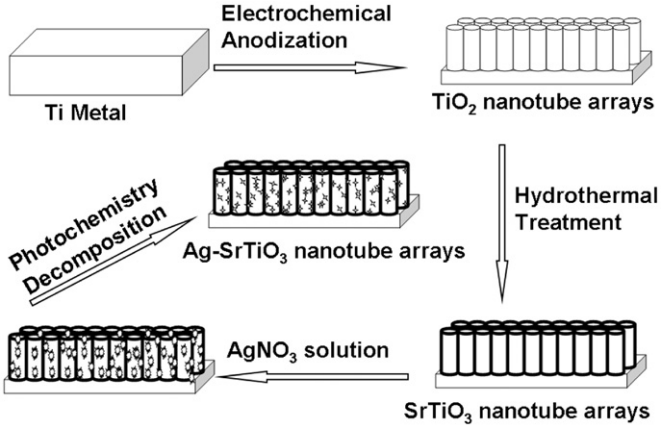

Fig. 8. Schematic diagram of the formation process of Ag–$SrTiO_3$ nanotube arrays.

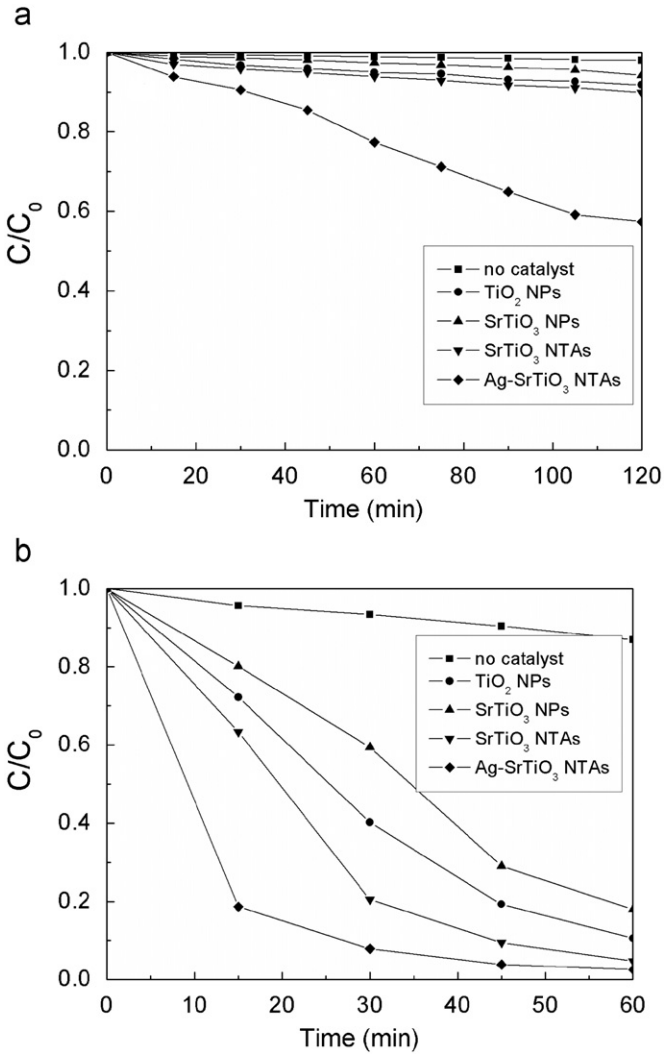

Fig. 9. Effect of pH on the degradation of methyl orange: (a) pH 7 and (b) pH 3. (NTAs and NPs represents nanotube arrays and nanoparticles, respectively.).

4. Conclusions

Ag–$SrTiO_3$ nanotube arrays were successfully prepared by hydrothermal method and photochemistry reduction method based on TiO_2 nanotube arrays. The SEM shows that $SrTiO_3$ nanotube arrays have highly ordered nanostructures with uniform diameter and the loaded Ag nanoparticles are uniformly dispersed on the nanotubes surface. The experiment results

indicate that Ag–$SrTiO_3$ nanotube arrays show an excellent photocatalytic performance for degradation of methyl orange. The enhancement of photocatalytic activity can be explained by Ag nanoparticle as an electron capture trap to prevent the recombination of electron–hole pairs effectively. Additionally, results of photocatalytic experiments indicate that an acidic conditon is very favorable for photocatalytic degradation of methyl orange.

Acknowledgments

This work was supported by National Natural Science Foundation of China (Grant nos. 50902040 and 50802021), Research Foundation for Personnel in Science and Technology Innovation of Harbin (2009RFQXG046), Science Foundation of Educational Commission of Heilongjiang Province (11541096) and Heilongjiang Province Science Foundation for Young Scholar (QC2010065).

References

[1] H.-J. Oh, J.-H. Lee, Y.-J. Kim, S.-J. Suh, J.-H. Lee, C.-S. Chi, Appl. Catal. B 84 (2008) 142–147.
[2] Y.B. Liu, B.X. Zhou, J. Bai, J.H. Li, J.L. Zhang, Q. Zheng, X.Y. Zhu, W.M. Cai, Appl. Catal. B 89 (2009) 142–148.
[3] N. Xiao, Z. Li, J. Liu, Y. Gao, Thin Solid Films 519 (2010) 541–548.
[4] A. Fujishima, K. Honda, Nature 238 (1972) 37–38.
[5] J.W. Liu, G. Chen, Z.H. Li, Z.G. Zhang, J. Int., Hydrogen Energy 32 (2007) 2269–2272.
[6] Z. Li, Y. Wang, J. Liu, G. Chen, Y. Li, C. Zhou, J. Int., Hydrogen Energy 34 (2009) 147–152.
[7] N. Xiao, Z. Li, J. Liu, Y. Gao, Mater. Lett. 64 (2010) 1776–1778.
[8] Y. Wang, Y. Huang, W. Ho, L. Zhang, Z. Zou, S. Lee, J. Hazard. Mater. 169 (2009) 77–87.
[9] Y. Xie, X. Zhao, Y. Li, Q. Zhao, X. Zhou, Q. Yuan, J. Solid State Chem. 181 (2008) 1936–1942.
[10] L. Kong, X. Lu, X. Bian, W. Zhang, C. Wang, J. Solid State Chem. 183 (2010) 2421–2425.
[11] V. Subramanian, R.K. Roeder, E.E. Wolf, Ind. Eng. Chem. Res. 45 (2006) 2187–2193.
[12] J. Zhang, J.H. Bang, C. Tang, P.V. Kamat, ACS Nano 4 (2010) 387–395.
[13] J.W. Liu, G. Chen, Z.H. Li, Z.G. Zhang, J. Solid State Chem. 179 (2006) 3704–3708.
[14] H. Zhang, X. Wu, Y. Wang, X. Chen, Z. Li, T. Yu, J. Ye, Z. Zou, J. Phys. Chem. Solids 68 (2007) 280–283.
[15] Y. Liu, L. Xie, Y. Li, R. Yang, J. Qu, Y. Li, X. Li, J. Power Sources 183 (2008) 701–707.
[16] X. Zhang, K. Huo, L. Hu, Z. Wu, P.K. Chu, J. Am. Ceram. Soc. 93 (2010) 2771–2778.
[17] G.K. Mor, K. Shankar, M. Paulose, O.K. Varghese, C.A. Grimes, Nano Lett. 5 (2005) 191–195.
[18] N. Lu, S. Chen, H. Wang, X. Quan, H. Zhao, J. Solid State Chem. 181 (2008) 2852–2858.
[19] S. Yoriya, M. Paulose, O.K. Varghese, G.K. Mor, C.A. Grimes., J. Phys. Chem. C 37 (2007) 13770–13776.
[20] J.M. Macak, M. Zlamal, J. Krysa, P. Schmuki, Small 3 (2007) 300–304.
[21] Y. Yang, X. Wang, C. Sun, L. Li, Nanotechnology 20 (2009) 055709.
[22] Y. Yang, X. Wang, C. Zhong, C. Sun, L. Li, Appl. Phys. Lett. 92 (2008) 122907.
[23] J.M. Macak, C. Zollfrank, B.J. Rodriguez, H. Tsuchiya, M. Alexe, P. Greil, P. Schmuki, Adv. Mater. 21 (2009) 3121–3125.
[24] Y.Y. Chen, B.Y. Yu, J.H. Wang, R.E. Cochran, J.J. Shyue, Inorg. Chem. 48 (2009) 681–686.
[25] S.K. Mohapatra, N. Kondamudi, S. Banerjee, M. Misra, Langmuir 24 (2008) 11276–11281.
[26] E. Stathatos, P. Lianos, P. Falaras, A. Siokou, Langmuir 16 (2000) 2398–2400.
[27] H. Ma, B. Wang, X. Luo, J. Hazard. Mater. 149 (2007) 492–498.
[28] I. Paramasivam, J.M. Macak, P. Schmuki, Electrochem. Commun. 10 (2008) 71–75.
[29] J.C. D'Oliveira, G. Al-Sayyed, P. Pichat, Environ. Sci. Technol. 24 (1990) 990–996.